IEEE Access
Multidisciplinary | Rapid Review | Open Access Journal

Date of publication xxxx 00, 0000, date of current version xxxx 00, 0000.

Digital Object Identifier xxxxxxxxxxxxxxx

Theoretical and Experimental Results for Multipactor Effect in Groove Gap Waveguide Bandpass Filters with Inductive Coupling Irises

ALEJANDRO JORGE-LÓPEZ [1], JOSÉ JOAQUÍN VAGUE [1], IRENE ASENSIO [1], ÁNGELA COVES [2], (Senior Member, IEEE), ÁNGEL A. SAN BLAS [2], MARIANO BAQUERO-ESCUDERO [1], (Member, IEEE), MÁRIAM TARONCHER [1], ANA VIDAL [1], (Member, IEEE), AND VICENTE E. BORIA [1], (Fellow, IEEE), (Member, IEEE)

[1]Departamento de Comunicaciones-ITEAM, Universitat Politècnica de València, 46022 Valencia, Spain (e-mail:ajorlop@iteam.upv.es; vboria@dcom.upv.es).
[2]Department of Communications Engineering-I3E, Universidad Miguel Hernández de Elche, 03202 Elche, Spain.

Corresponding author: Alejandro Jorge-López (e-mail: ajorlop@iteam.upv.es).

Manuscript received MM DD, 202Y; revised MM DD, YYYY; accepted MM DD, 202Y. Date of publication XXXXX XX 202x. This work has been funded by the Ministerio de Ciencia, Innovacion y Universidades (Spanish Government) through the Subprojects C41 and C43 of the R&D Projects PID2022-136590OB (under grant AEI/10.13039/501100011033/FEDER, UE) and TED2021-129196B (under grant 10.13039/501100011033/Unión Europea NextGenerationEU/PRTR), and in part by Conselleria de Educación, Universidades y Empleo, Generalitat Valenciana under Project CIAICO/2021/055.

ABSTRACT This article presents the theoretical study and experimental validation of the multipactor (MP) effect in bandpass filters implemented in groove gap waveguide (GGW) technology. Such filters are based on rectangular cavities and inductive coupling irises, whose optimized dimensions (widths and lengths) are fixed between rows of metal pins. For the effective design of the considered GGW filter, an equivalent counterpart in standard rectangular waveguide (RW) technology will be first studied, using very efficient tools for computing its electrical response and MP discharge breakdown levels. Two prototypes of the GGW and RW bandpass filters, designed to operate at 17.5 GHz (for Ka-band satellite downlink applications), are manufactured for validation and comparison purposes. Both of them are made of aluminium material, whose properties (in terms of secondary electron emission) have also been measured, as well as considered in the prediction of MP threshold levels using available software tools. Proceeding in this way, an outstanding matching between all simulated and experimental results of the MP effect has been achieved.

INDEX TERMS Bandpass filters, groove gap waveguide, inductive irises, multipactor effect, rectangular waveguide.

I. INTRODUCTION

Multipactor (MP) is a potentially harmful discharge effect that occurs inside microwave components operating under high-vacuum conditions. In these situations, electrons allocated inside the device can be accelerated by electromagnetic (EM) fields of high amplitude (power level), pushing them (in a synchronized way) towards the surrounding surfaces, where they may impact with enough energy to extract more (and more) secondary electrons [1], [2]. When all these conditions are met an electron chain discharge effect is produced, whose features (intensity and dynamics) strongly depends on the surface material property known as the Secondary electron Emission Yield (SEY) [3]. The cited resonant discharge inside the MP-affected component creates an electrical short-circuit that generates signal harmonics, decreases the signal-to-noise ratio (SNR) and, eventually, causes physical damages [4]–[6]. Thus, MP discharges will impact negatively in many practical applications dealing with high-power microwave signals inside high-vacuum operating components, as it occurs in the output stage of satellite communication payloads [7]–[9] and in particle accelerators [10].

As it is well known [1], [2], the MP breakdown power (or MP threshold level) is directly related to the product of the operating frequency (GHz), and the gap distance (mm) between two (usually metallic) surfaces of the microwave component. This dependence is clearly observed in the corresponding MP

susceptibility charts, that were firstly obtained for parallel-plate waveguide geometries using analytical models [1] and empirical data [11]. Later on, several methods have been used for the study of the MP effect in widely common high-frequency technologies, such as rectangular, circular and ridge waveguides [12]–[14], as well as coaxial and planar (microstrip) transmission lines [15], [16]. More recently, in order to estimate the MP threshold levels of advanced microwave hardware used in real applications, fast approximate techniques based on equivalent circuits, as well as more accurate (and time-consuming) simulators for particles driven by electromagnetic (EM) fields, are also being employed [17].

A general trend in modern communications systems, and more specifically for satellite applications, is to increase the channel bandwidth (in order to support greater transmission rates) thus leading to higher operational frequencies. Indeed, this is the case of the high throughput satellite (HTS) systems [18], presently transmitting high-power signals at the far-end of the classical Ku-band (17 GHz and above), also catalogued as the Ka-band for space communication downlinks [19]. A recently emerged technology for the practical implementation of these high-frequency components, relies upon the use of groove gap waveguides (GGWs) [20]. For instance, recent results on GGW filters and diplexers at Ku- and Ka-band can be found in [21]–[25].

In this GGW solution, the tight metallic contact between the top lid and the body, which is always required when using the standard rectangular waveguide (RW) technology, is widely relaxed. To this end, periodic rows of pins (providing a high-impedance condition to the top lid [26]) are introduced in the GGW body, so the perfect metallic contact between the two parts is not anymore needed [27], [28]. Then, even if a small physical gap (of a few tens of μm) is present (due to inevitable mechanization errors) between the top lid and its body, the GGW technology provides top quality components without EM leakage (see recent examples at Ka-band and above in [29], [30]).

However, a potential drawback of GGWs (more likely when used in Ku- and Ka-band applications), is that real components may suffer from high-power discharges (in particular MP breakdown) within the cited tiny gaps between metallic surfaces (top cover and body), thus limiting their power-handling capabilities. Nevertheless, there are only two very recent contributions addressing the problem of electronic discharges in GGW technology so far. The first one is focused on the corona (or gas breakdown) effect that, contrarily to MP, requires of a certain pressure level inside the device [31]. On the other hand, the second work is focused on studying MP discharges, but just considering a very simple E-plane GGW transformer operating in the upper-end side of the X-band (10-12 GHz) [32]. Therefore, there is a complete lack of theoretical and experimental studies of the MP effect in more realistic GGW components (such as filters) operating at higher frequencies (e.g. in the Ka-band), which are aimed to be fully addressed in this article. A comparison of the GGW filter results with those for a counterpart in standard

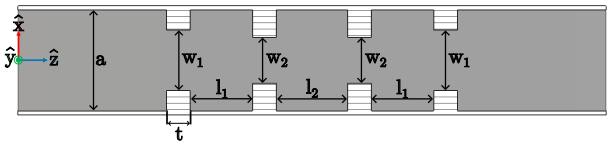

FIGURE 1. **Geometry (top-view) of an inductive filter in RW technology (a= 12.95 mm, w_1= 7.73 mm, w_2= 5.86 mm, l_1= 8.05 mm, l_2= 9.18 mm and t= 3 mm, for a bandpass response of center frequency 17.5 GHz and relative bandwidth 3.85%). The height of the structure is 6.477 mm (for WR-51 ports) and 3 mm (for the optimal solution).**

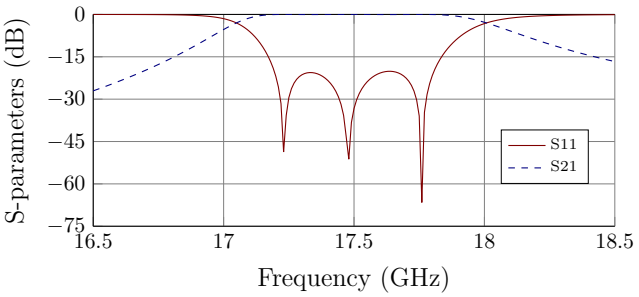

FIGURE 2. **Electrical response (S-parameters) of the RW inductive filter.**

RW technology is also performed, in order to confirm they can be alternative technological solutions.

Thus, in this paper we will consider a GGW filter (with a bandpass response of 675 MHz centered around 17.5 GHz) based on cavities coupled through inductive irises. For its complete design process (both in terms of electrical response and MP effect), the filter counterpart in RW technology will be first studied, using efficient software tools based on modal analysis and MP theoretical models specially suited for RW geometries. Proceeding in this way, the maximum value of the filter height (compatible with the MP breakdown power levels that can be measured in the available experimental facility) will be found, hence also considering a more realistic component in terms of GGW height (with a greater value than the reduced one for the X-band transformer in [32]). The next sections of this paper cover all cited contents related to the electrical design, and MP effect analysis, of the proposed GGW filter and its RW counterpart. Experimental results for both filter prototypes, obtained from a test campaign performed at the High Power Laboratories of the European Space Agency (ESA) and the Val Space Consortium (VSC) [33], are compared and properly discussed. Finally, the main conclusions of this work are briefly outlined.

II. MULTIPACTOR ANALYSIS OF INDUCTIVE FILTERS IN RECTANGULAR WAVEGUIDES

In this section, we detail the complete design procedure of an equivalent inductive filter in RW technology, that will be used as a starting point for implementing the same topology with GGWs. In addition, efficient modelling techniques of the MP effect for RW geometries will be also employed, thus substantially reducing the computational effort of existing commercial tools (based on more elaborated methods) for dealing

with GGW technology. As it will be shown, this approach will reveal extremely useful for the considered GGW filter, since its realistic height value (compatible with the existing power limits in the experimental facility) involves MP modes of very high order (whose accurate analysis with the cited commercial tools takes prohibitive simulation times).

Inductively-coupled RW filters are based on the cascade connection of RWs (all with the same height, but with different width values), whose geometry (an H-plane cut of the 3-D component) with the main dimensions for design purposes can be seen in Fig. 1. They are considered a classical filtering structure, widely used in satellite communication systems, whose accurate synthesis and design relies on well-established techniques [34], [35]. For this work, a third-order RW filter, with a Chebyshev response centered at 17.5 GHz (Ka-band) with a relative bandwidth of 3.85% (around 675 MHz), has been designed using the automatic synthesis tool of FEST3D (now part of CST Studio Suite, Dassault Systèmes [36]), which is specially suited for the considered inductive topology. The resulting dimensions of such RW filter are included in the caption of Fig. 1, whereas its simulated electrical response (matching the required specifications) is shown in Fig. 2.

To feed the designed inductive filter, we have first considered a standard WR-51 RW (of size 12.954 mm × 6.477 mm), thus involving a constant value of 6.477 mm for the height of all involved waveguides. For such a nominal height value, as it was discussed in [37], the MP breakdown power levels will be of several tens of kW (well beyond the maximum value available in the experimental facility [33], which is around 5 kW for the considered Ka-band frequency range). Thus, the height value must be properly reduced (to accommodate the previous restriction), but without compromising other relevant features (e.g. insertion losses and quality factor) of a realistic filter solution. For this purpose, an effective iterative procedure (based on very efficient MP analysis models) will be used to find the optimal height solution.

For the initially designed RW filter, we can see (Fig. 3) that the maximum value of the electric field magnitude (computed at the central frequency of its bandpass response) is located in the center of the second (central) cavity. Due to the particular geometry of inductive filters (invariant with height), the pattern for the electric field distribution is kept constant for any height value. Therefore, the same location for having a MP discharge (i.e. the RW implementing the central resonator) can be considered in the iterative design process of the filter height. Additionally, the same values for all dimensions of the inductive filter (those in the caption of Fig. 1) also remain fixed at all stages of the procedure detailed next.

Thus, for each potential value of the filter height, we will first compute the MP threshold power of a uniform section of the RW implementing the central cavity (P_{TH}), using an efficient model specially built for that purpose. To this end, a MP analysis tool based on the effective-electron model (originally developed and validated with partially dielectric-loaded RWs, see [38] and [39]), has been suited for empty standard

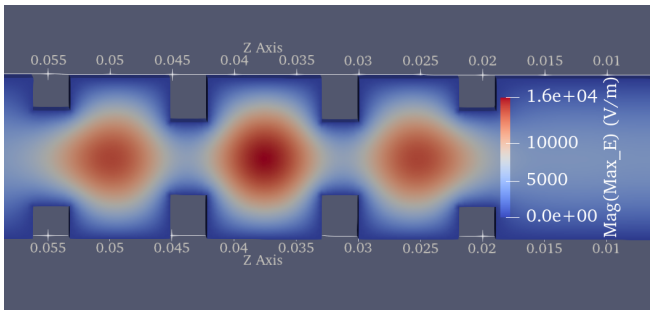

FIGURE 3. Electric field distribution in the RW inductive filter computed at 17.5 GHz (with levels scaled for an input power level of 1 W and a height of 6.477 mm).

RWs (named as Numerical-RW in this article). Additionally, a simplified version of the previous tool (based on the analytical resolution of the effective electron trajectory) has also been developed for this work (called Analytical-RW from now on). Even though both models can solve the MP discharge effect in empty RWs very efficiently, the second version is extremely fast, and particularly suitable for the proposed iterative procedure. It is based on neglecting the influence of the magnetic field components of the RW fundamental mode, which was also tried (although partially, and not leading to a completely analytical solution) by other authors before [12]. This approach is valid when calculating electron trajectories under non-relativistic velocities, which is the usual case in microwave hardware for satellite applications.

Since MP is a driven-voltage effect, we can easily relate the previously computed P_{TH} value with the peak voltage level (V_{TH}) required for such a discharge, using the well-known relationship [17]:

$$V_{TH} = V_{1W}\sqrt{\frac{P_{TH}}{P_{1W}}} = V_{1W}\sqrt{P_{TH}} \tag{1}$$

where V_{1W} is the peak voltage in the critical gap of the uniform RW (which is located at the waveguide center, where the TE_{10} mode electric field is maximum), for a mean power level of 1 W at the waveguide input port (P_{1W}= 1 W).

However, we finally need to know the MP threshold power at the input port of the whole inductive filter (P_{FTH}), that will be lower than the previous one (P_{TH}) due to the voltage magnification effect originated in the resonant cavities of bandpass filters [7]. In this case, we can easily compute the value of P_{FTH} as follows:

$$P_{FTH} = P_{F1W}\left(\frac{V_{TH}}{V_{F1W}}\right)^2 = P_{TH}\left(\frac{V_{1W}}{V_{F1W}}\right)^2 \tag{2}$$

where V_{F1W} is the value of the peak voltage in the middle of the central resonant cavity of the filter (where, according to Fig. 3, the MP discharge will be generated), but now for a 1 W mean power level at the filter input port (P_{F1W}= 1 W).

It must be noted that the values of V_{1W} and V_{F1W} (for each different value of the waveguide height) are also efficiently computed with the software tool FEST3D (used before for the automated design of the inductive filter). Applying this

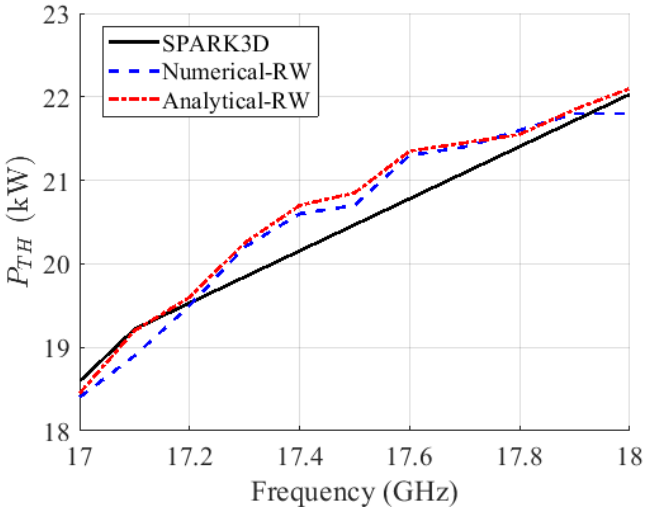

FIGURE 4. MP threshold power levels for the WR-51 RW with a height of 3 mm, computed with SPARK3D (solid line) and with the two efficient MP tools for RWs (Numerical-RW and Analytical-RW with dashed and dotted lines, respectively).

TABLE 1. Standard SEY data for aluminium (Al) material.

Material	E_{max} (eV)	E_1 (eV)	δ_0	δ_{max}
Al (ECSS2020 [40])	276.00	17.00	0.80	2.92

procedure to our case, iteratively, an optimal value of 3 mm for the RW filter height is found after completing few simple steps (where very efficient electrical and MP analysis tools have been employed).

Next, we will check that the two efficient MP analysis tools used in this work (the Numerical-RW and the Analytical-RW ones) do also provide accurate results. For this purpose, we have first considered a uniform RW section of size 12.954 mm × 3 mm (i.e. with the width of the standard WR-51 RW and the optimum height value that was found), made of aluminium material (whose standard SEY data, from [40] and compiled in Table 1, are used). For validation of the P_{TH} values obtained for the cited RW, we have also used the well-known software tool SPARK3D (v. 2023, Dassault Systèmes), based on a more elaborated (but less efficient) algorithm for tracking electrons driven by the real EM fields inside the component. Fig. 4 shows the three sets of previous results for 11 points in the frequency range from 17 GHz to 18 GHz (where the whole pass-band of the RW inductive filter is included), that were obtained with an Intel(R) Xeon(R) computer at 2.10 GHz with 64 GB RAM. As can be seen, a very good agreement between all MP results is achieved.

In order to get the results with SPARK3D (used as reference for our comparative study), 10 000 initial electrons were homogeneously distributed within the uniform RW section, thus involving 24 hours for the complete simulation of MP effect at each frequency point. This extremely large computational effort is directly related to the very high order of the MP mode excited in the uniform RW (that SPARK3D has

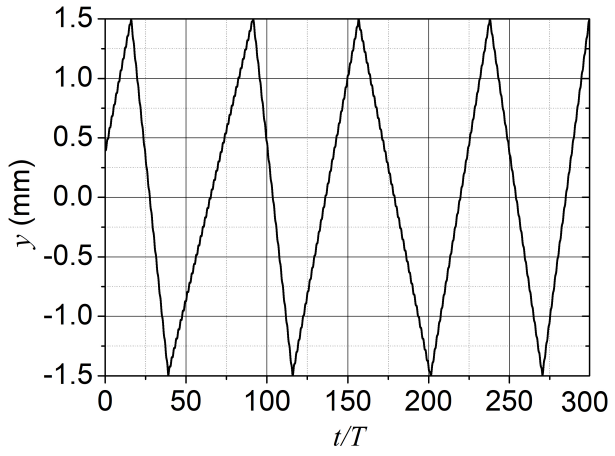

FIGURE 5. Time-evolution of an effective electron trajectory (along the y-coordinate) for the WR-51 RW with a height of 3 mm (excitation signal of P_{TH} = 21 kW at f = 17.5 GHz), computed with the very efficient Analytical-RW tool.

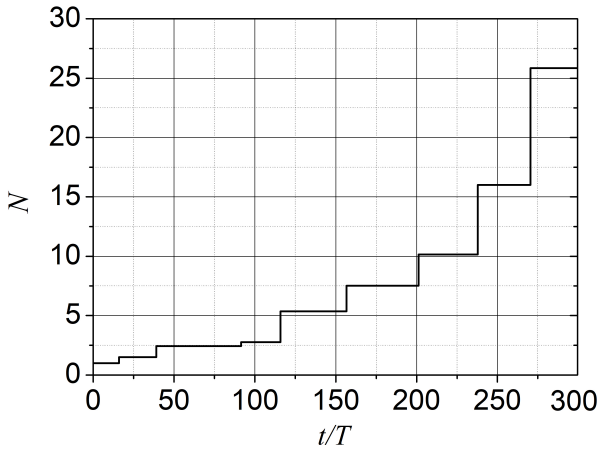

FIGURE 6. Time-evolution of the average value N for the WR-51 RW with a height of 3 mm (excitation signal of P_{TH} = 21 kW at f = 17.5 GHz), computed with the very efficient Analytical-RW tool.

predicted to be equal to 73), as it can be expected for a value of the frequency-gap product ($f \times d$) of 52.5 GHz × mm, considering the central frequency of 17.5 GHz. Using the two efficient tools for the MP effect analysis, properly configured as detailed next, we have also computed a very close value (of 71) for the order of the excited discharge mode. These results confirm that a large number of half-cycles of the sinusoidal excitation signal must be considered to reach reliable MP results. Thus, longer temporal simulation intervals will be involved, which discourages the use of very accurate (but less computationally efficient) commercial tools in this case.

Both the Numerical-RW and the Analytical-RW tools have computed the P_{TH} values of Fig. 4 following the same statistical approach. For each power value, the trajectories of 36 effective electrons, with initial phases of the driving

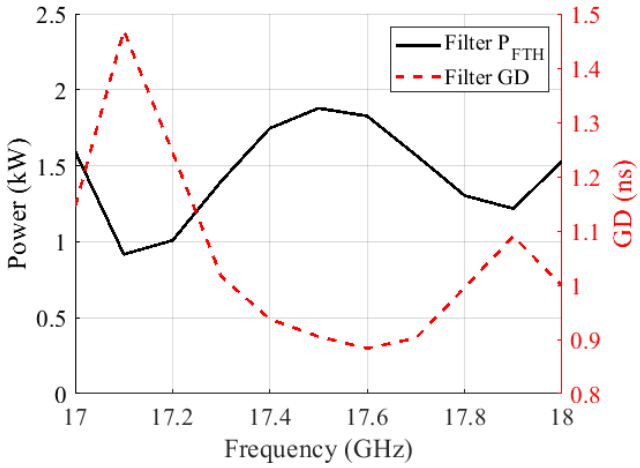

FIGURE 7. MP threshold power levels at the input port of the filter in WR-51 RW with a height of 3 mm (P_{FTH} in kW, left-hand side scale), and filter group delay (GD in ns, right-hand side scale), computed with the Analytical-RW tool (P_{TH} values) and FEST3D, respectively.

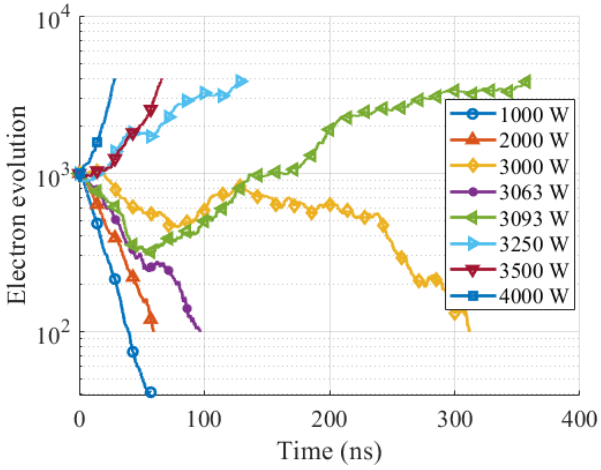

FIGURE 8. Electron population evolution for the MP analysis (at 17.5 GHz) of the filter in WR-51 RW with a height of 3 mm, performed with SPARK3D.

electric field uniformly distributed between 0° and 360°, are computed. They are launched from the center of the RW (i.e. at $x = 0$ and $z = 0$ according to the geometry of Fig. 1), and from random positions between y= -1.5 mm and y= 1.5 mm (for the considered height of 3 mm). After 300 periods ($T = 1/f$) of the high-frequency excitation signal, for all simulated trajectories, the average value of the final population of electrons (N) is used to determine (if such a value is above 1) that a MP discharge has occurred.

For the RW under study, considering f= 17.5 GHz and P_{TH}= 21 kW (above the MP threshold for such frequency value, see Fig. 4), an effective electron trajectory and the accumulated population of electrons are shown in Fig. 5 and Fig. 6, respectively. Only results obtained with the Analytical-RW tool (computed in just 2 minutes) are included, since those provided by the Numerical-RW approach (in 55 minutes) are practically superimposed. From the results of Fig. 5, the value for the order of the excited MP mode can be directly estimated (obtaining a value around 71, rather similar to the SPARK3D reported value of 73). However, the Analytical-RW tool has also provided accurate MP results with very reasonable computational efforts.

Next, using the values of P_{TH} provided by the Analytical-RW tool (see Fig. 4) in eq. (2), together with figures for V_{1W} and V_{F1W} computed before, we have finally estimated the levels of P_{FTH} (the MP threshold power at the input port of the RW inductive filter), which are displayed in Fig. 7. They are shown again in the whole frequency range between 17 GHz and 18 GHz, where the filter bandwidth (675 MHz) is fully comprised, thus confirming that all values of P_{FTH} for the selected optimal height (i.e. 3 mm) remain below the maximum breakdown level occurring at 17.5 GHz (the filter center frequency). This evolution of the P_{FTH} curve (see Fig. 7) is entirely aligned with the electrical response of the designed RW filter (also represented in Fig. 7 through the group delay (GD) parameter). As can be seen, the minimum values of P_{FTH} are coincident with the peaks (maximums) of the filter GD (where the time-averaged stored energy (TASE) in the filter structure is also maximized), which is fully consistent with previous works relating all these concepts [17]. From results in Fig. 7, it is confirmed that the RW filter (of 3 mm height) is suitable for performing MP measurements in the selected facility (since the P_{FTH} values, always below 2 kW, are far away from the 5 kW offered by the available laboratory equipment).

Finally, before proceeding with the refined design process (and MP analysis) of the GGW bandpass filter, making use of the previous results for the RW counterpart, we will check that the threshold power results of Fig. 7 are broadly reliable. For this purpose, we have computed the value of P_{FTH} for the RW filter (at 17.5 GHz) using the accurate commercial tool SPARK3D, that will resolve all simplifications exploited in the two efficient MP analysis tools detailed above. Fig. 8 shows the electron population evolution (inside the designed RW filter) for the automated power sweep performed by SPARK3D, which predicts a value of 3093 W for P_{FTH} (higher than the maximum value at 17.5 GHz in Fig. 7, but still distant enough from the 5 kW limit of the experimental facility). Accordingly, we can now transfer the inductive RW filter solution to the GGW technology, as will be detailed in next section, and then perform an accurate MP analysis of the more complex GGW filter geometry.

III. MULTIPACTOR ANALYSIS OF INDUCTIVE FILTERS IN GROOVE GAP WAVEGUIDES

Once the RW inductive bandpass filter has been deeply studied (see previous section), we will proceed with its practical implementation in GGW technology (see the 3-D view of the proposed topology in Fig. 9 (a)), and the corresponding MP analysis. For these purposes, more accurate (but less efficient) software tools (such as the high-frequency EM simulation solver of the aforementioned CST Studio Suite [36], and the

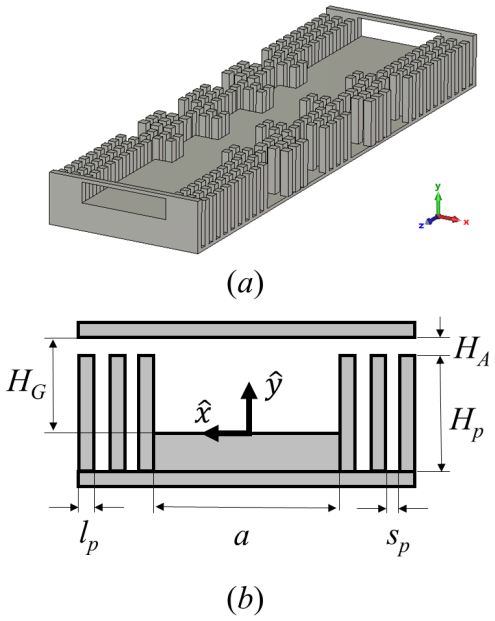

FIGURE 9. 3-D view of the inductive bandpass filter in GGW technology in (a), and 2-D geometrical representation of each GGW in (b).

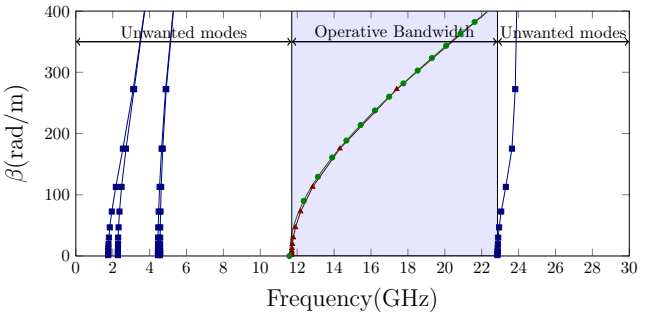

FIGURE 10. Dispersion diagram of the GGW with size 12.954 mm × 3 mm, pins of l_p= 1.02 mm , s_p= 0.96 mm and H_A= 20 μm (unwanted modes with solid lines and fundamental mode with triangles marks), and of the equivalent RW (fundamental mode with circle marks).

electrons tracking code SPARK3D) will be needed to cope with the more intricated GGW geometry. To alleviate the corresponding computational burdens, we will rely on the available RW inductive solution as it is described next.

First, each RW (with the optimal height of 3 mm found in section II) of the inductive filter is directly replaced with its corresponding GGW counterpart (whose geometrical details are given in Fig. 9 (b)). The same values for the width, height and length of all RWs of the filter conceived in section II (which are collected again in Table 2) are initially chosen for the corresponding GGWs (where all their heights are kept constant, i.e. H_G= 3 mm in Fig. 9 (b)). Regarding the periodic bed of pins (of square cross-section with size l_p separated a distance equal to s_p, see Fig. 9 (b)), it has been properly designed for implementing the high-impedance surface of the GGW technology, thus obtaining l_p= 1.02 mm and s_p= 0.96 mm for a nominal height value of H_p= 6.477 mm. Such a textured surface, together with the top metal lid, prevent any potential leakage of EM energy through the GGW lateral sides [26], [27]. Additionally, as will be shown below, each pair of equivalent RWs and GGWs will behave practically identical in terms of the dispersive behavior of their respective fundamental modes [41].

In this work, the zero-gap GGW realization (with H_A in Fig. 9 (b) ideally equal to 0 μm) is used. For Ka-band applications [29], it has alleviated the fabrication process of the classical GGW approach, where fixed non-zero values of H_A (about several hundreds of μm [41]) must be kept. The zero-gap solution is also very convenient to avoid undesired MP discharges that, as thoroughly studied with uniform GGW sections [32], can be easily triggered at very low power levels in the cited larger air gaps of the classical GGW case. However, due to mechanical tolerances (that can be guaranteed with standard fabrication techniques used in previous works, see [29] and [32]), very small air gaps (with values of H_A below 20 μm) may be present in the produced pieces. Therefore, it has to be verified that such more realistic GGWs (considering in Fig. 9(b) that $H_A = 20\,\mu$m and $H_p + H_A$= 6.477 mm) do not deviate (in terms of electrical response and MP discharge) from the ideal zero-gap case ($H_A = 0\,\mu$m).

Both the proposed equivalence (in electrical terms) of the GGW and RW counterparts stated above, as well as the negligible effect of fabrication tolerances for the GGW case (i.e. $H_A \leqslant 20\,\mu$m), are first warranted. For this purpose, the dispersion diagrams of both waveguide implementations (in particular those of size 12.954 mm × 3 mm, used in the ports and resonant cavities of the two filters, and with $H_A = 20\,\mu$m for the GGW real version) are computed using the eigenmode solver of CST Studio Suite. As can be seen in Fig. 10, apart from some additional unwanted modes that appear in the GGW case (e.g. the ones at low frequencies due to the small, but non-zero, value of 20 μm considered for H_A), both fundamental modes do have overlapped dispersion responses in the same operational bandwidth. Thus, the proposed replacement of each RW in the original filter by its corresponding GGW implementation (with $H_A \leqslant 20\,\mu$m), is well justified in the single-mode frequency range of both waveguides.

In terms of the MP discharge, an empirical verification that such effect will not be produced (with very low power levels) in the cited small air gaps (of height values $H_A \leqslant 20\,\mu$m), is performed using the well-known susceptibility charts of parallel-plate geometries. For the considered range of realistic values for H_A, and at frequencies in the operational bandwidth of the GGW filter (below 18 GHz), the frequency-gap product ($f \times d$) will always meet that $f \times d \leqslant 0.36\,\text{GHz} \times \text{mm}$. Based on the standard susceptibility charts for aluminium material [11], and for such low values of the $f \times d$ term, it can be noticed that no MP discharge (of any order) will ever occur. As a result, we can also replace RWs by real GGW realizations (with $H_A \leqslant 20\,\mu$m) without affecting the MP response of the inductive filter (as it will be also checked

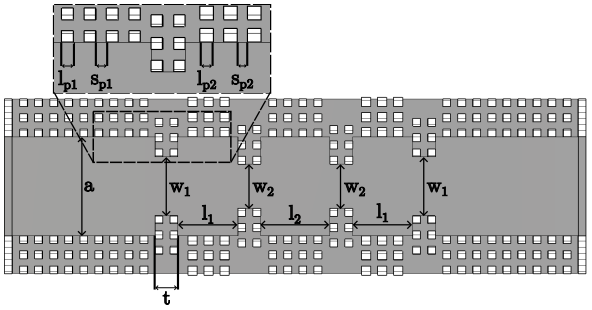

FIGURE 11. Geometry (top view) of the inductive filter in GGW technology, with all dimensions used for design purposes (note the symmetry of the structure regarding the central resonator). The height of GGWs is H_G= 3 mm.

TABLE 2. Optimized values for dimensions (all in mm) of the RW and GGW inductive filters.

Dimension	a	w_1	l_1	w_2	l_2	t
RW	12.95	7.73	8.05	5.86	9.18	3.00
GGW	12.95	7.71	7.89	5.80	9.07	3.00

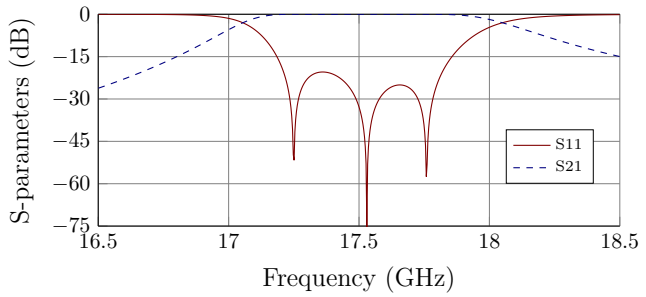

FIGURE 12. Electrical response (S-parameters) of the GGW inductive filter.

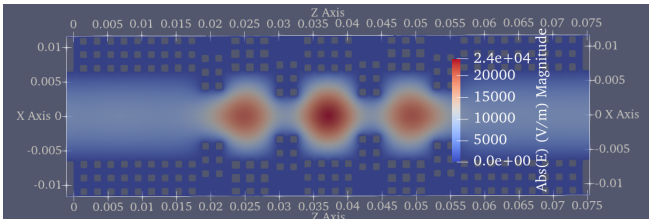

FIGURE 13. Electric field distribution in the GGW inductive filter, calculated at 17.5 GHz (with levels scaled for an input power level of 1 W and height H_G= 3 mm).

below with more accurate simulations of the whole structure).

The previous results do also sustain that it is an optimal choice to use, as initial values for all dimensions of the GGW filter to be designed, those found for the RW case (whose data are compiled in the first row of Table 2). Proceeding in this way, and supported by CST Filter Designer 3D tool (also part of CST Studio Suite), the entire design process of the inductive bandpass filter in zero-gap ($H_A = 0\,\mu$m) GGW technology is completed after few steps. All geometrical dimensions involved at the filter design stage are shown in Fig. 11, where it can be seen that two different sets of square pins have been employed. Most of them are those pins used before in the GGW body (i.e. with $l_{p1} = l_p = 1.02$ mm and $s_{p1} = s_p = 0.96$ mm), whereas the lateral pins of the first and third filter cavities do have $l_{p2} = 1.2$ mm and $s_{p2} = 0.9$ mm. These latter values were selected, similarly as in [42], to best fit the requested optimal value for the length of such two resonators.

As it can be observed in Table 2, the optimal values of all dimensions for both RW and GGW filters are rather similar, which confirms that the design strategy followed with the GGW case (starting from the optimal solution for the RW counterpart) is indeed very efficient. By doing so, a huge amount of computational efforts (related to the accurate simulations, with CST Studio Suite, of the more complex GGW structure) has been saved. A satisfactory bandpass response, fully compliant with the filter specifications in terms of central frequency and bandwidth, is also achieved (see Fig. 12). These results also remain stable if some tiny air gaps were present (due to minor fabrication errors) above the metallic pins.

Once the zero-gap GGW filter is successfully designed, we will perform an accurate MP analysis using the SPARK3D software tool at the central frequency of 17.5 GHz, and considering the SEY data of aluminium in Table 1 (see previous section). For the requested simulations, the driving EM fields have been computed with CST Studio Suite, showing the distribution (along the filter geometry) of the electric field magnitude in Fig. 13. As can be observed, the maximum value is clearly located in the center of the second (central) GGW cavity, thus confirming that the MP discharge will be generated in a very similar location to the one for the RW case (see Fig. 3). In fact, the predicted value for the MP threshold power of the GGW filter is 3188 W (see SPARK3D results in Fig. 14), which is very close (slightly higher) to the result for the equivalent RW filter (of 3093 W, as stated in section II). Additional MP simulations of the same GGW filter (considering now $H_A \leqslant 20\,\mu$m) have confirmed very similar threshold power levels, as well as that the corresponding discharges were kept in the central filter resonator (and not in the included small air gaps).

However, if the desired tolerances are not met (and $H_A > 20\,\mu$m), the unwanted MP effect may be located in the larger air gaps, and with substantially reduced threshold power levels. This highly dangerous MP event was already addressed in a previous study, that was performed in [32] with other GGW uniform sections (of smaller height equal to 0.8 mm, and operating at the lower frequency of 11 GHz). In such a case, it was obtained that air gaps of height 50 μm and above should be certainly avoided. However, for the GGW filter just designed and $H_A = 30\,\mu$m , the analysis results of SPARK3D clearly reveal (as can be seen in Fig. 15), that an undesired MP discharge is generated (with a very low power level of just 29 W) in the small gaps above pins.

When comparing the previous figure (limit value of 30 μm for H_A) with the one (of 50 μm) for the related study performed in [32], it must be taken into account that different op-

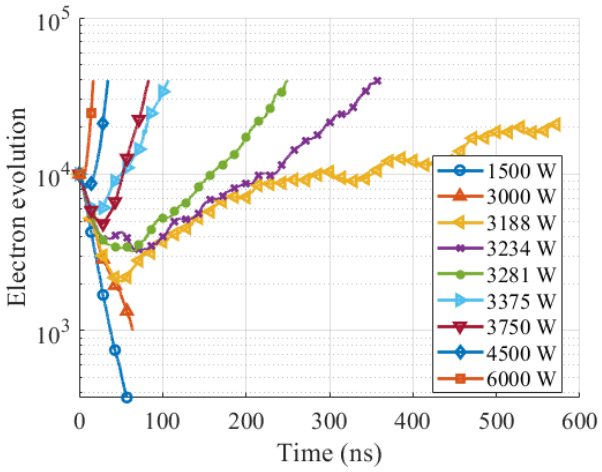

FIGURE 14. Electron population evolution for the MP analysis (at 17.5 GHz) of the filter in GGW technology (with H_C= 3 mm), performed with SPARK3D.

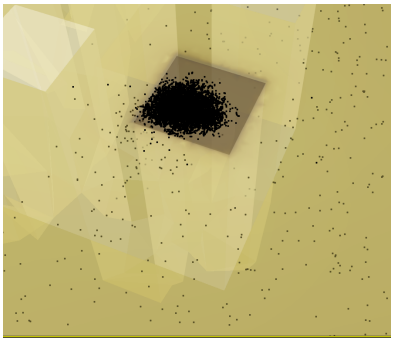

FIGURE 15. Electron cloud distribution of a MP discharge (with an input power of 29 W at 17.5 GHz) inside the GGW filter, located in a small air gap (of $H_A = 30\ \mu m$) between metal pins and the top lid.

erational frequencies were involved in each case (17-18 GHz for the GGW filter, and 10-12 GHz for the GGW transformer of [32]). Accordingly with MP susceptibility charts, in order to stay safe of MP discharges at low enough values of $f \times d$, smaller air gaps will be needed in GGW structures operating at higher frequency bands (as it is the case of the considered Ka-band filter). Experimental results in next section will, hopefully, confirm that the in-house facility used to fabricate the GGW filter prototype (with tolerances below the cited limit of 20 μm), is accurate enough for completing the MP study on inductive filters for Ka-band satellite applications.

IV. EXPERIMENTAL RESULTS AND DISCUSSION

The two RW and GGW filters designed before (sections II and III) have been manufactured in aluminium, using an in-house computer numerical control (CNC) milling technique (which provides the required accuracy of 20 μm). As can be seen in Fig. 16, they consist of a body (with all geometrical details of each filter prototype) and a smooth top metal lid. In order to measure both filters, since their input and output ports have a height of 3 mm, E-plane tapered transformers for matching such ports to standard WR-51 RWs (with a height

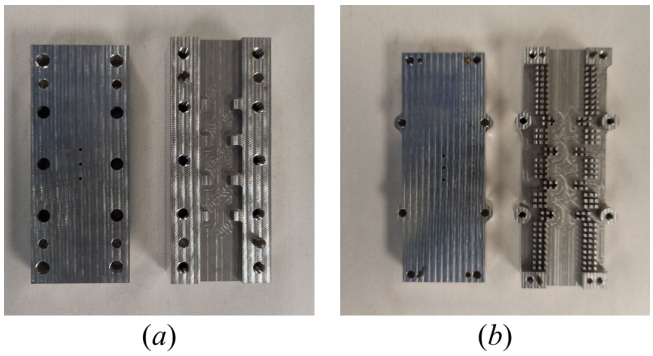

FIGURE 16. Manufactured prototypes of the inductive filters in RW (a) and GGW (b) technologies.

TABLE 3. Comparative data for simulated and measured bandpass responses of the RW and GGW inductive filters.

Filter	f_o (GHz)	BW (MHz)	BW (%)
Simul. RW	17.505	675	3.85
Meas. RW	17.415	710	4.01
Simul. GGW	17.513	675	3.85
Meas. GGW	17.334	728	4.19

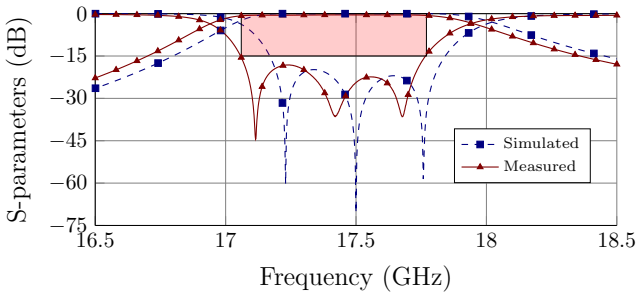

FIGURE 17. Simulated (with squares) and measured (with triangles) electrical response (S-parameters) of the RW inductive filter (including the E-plane tapered transformers).

value of 6.477 mm) are also built, after being designed as recently discussed in [43].

Comparisons between the simulated and measured results of the RW and GGW filter prototypes are shown in Fig. 17 and 18, respectively. A summary of the most relevant data of both sets of responses, i.e. their center frequencies and bandwidths (defined where return losses are above 15 dB), is found in Table 3. As can be noticed, minor deviations between all simulated and experimental results are generally observed. Among them, there is a frequency shift of 170 MHz (below 1% in relative terms) between both GGW filter responses, which can be attributed to the mechanical tolerances (of 20 μm) reached with the employed in-house fabrication technique. Nevertheless, since the measured return loss levels are below 15 dB in the slightly shifted in-band responses, it will be possible to perform the MP study (analysis and, in particular, testing) of both filter units. In this case, such results will be obtained at the frequency of 17.4 GHz, where the pass-bands of the two fabricated prototypes are actually centered.

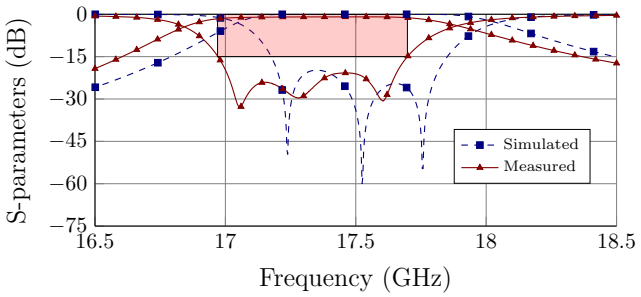

FIGURE 18. Simulated (with squares) and measured (with triangles) electrical response (S-parameters) of the GGW inductive filter (including the E-plane tapered transformers).

TABLE 4. Standard and measured SEY data for aluminium (Al) material.

Material	E_{max} (eV)	E_1 (eV)	δ_0	δ_{max}
Al (ECSS2020 [40])	276.000	17.000	0.800	2.920
Al (measured)	246.500	16.154	0.903	2.485

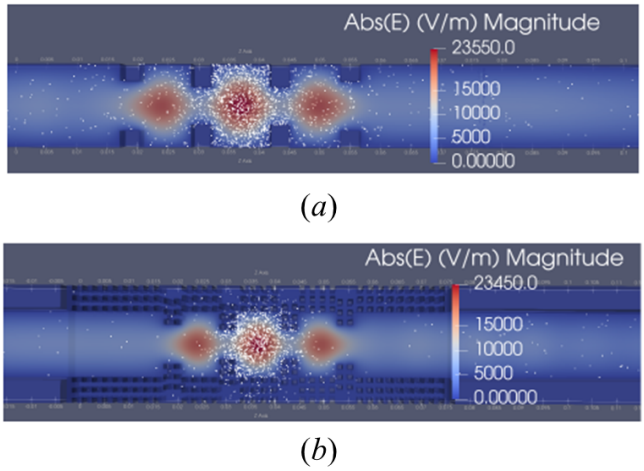

FIGURE 19. Zoomed views of the electron clouds in the RW (a) and GGW (b) filters, at 17.4 GHz and for the corresponding MP threshold levels (measured SEY data). The electric field distributions (levels scaled for an input power of 1 W) are also shown.

TABLE 5. Simulated (SPARK3D) and measured results (MP threshold levels) for RW and GGW filters at 17.4 GHz.

Model - Experiment	MP threshold (W)
RW simulation (ECSS2020 SEY)	3023.35
RW simulation (measured SEY)	3445.23
RW MP test	3424.50
GGW simulation (ECSS2020 SEY)	3163.98
GGW simulation (measured SEY)	3679.61
GGW MP test	3468.30

For the intended comparative study of the MP response of both (RW and GGW) filters, the cited software tool SPARK3D is used to compute, with high accuracy, the corresponding power threshold levels. The driving EM fields will be obtained, for the two filter structures (including the required input and output transformers), running CST Studio Suite in the frequency-domain. In order to simulate the MP effect more realistically, in addition to use the SEY standard data for the involved material (aluminium) [40], as it is usually done (see sections II and III), measured results for such key material property will be also employed. To this end, the corresponding experimental SEY data have been obtained, from one metallic top lid of the filters, through measurements performed at the European High Power Space Materials Laboratory [33]. These measured values for the real aluminium sample are collected, together with the standard data from [40], in Table 4. From the practical meaning of all SEY parameters in Table 4 (see details in [44]), it can be anticipated that different threshold values for the MP threshold levels will be obtained (in particular higher values when measured SEY data are considered in simulations).

After all MP simulations (for both sets of filters and available SEY data) are performed, we can check (from the corresponding threshold power levels displayed in Table 5), that both technologies (when considering the same set of SEY data) do provide similar values. Such similarity is based on the effective concentration of the EM fields in the central region of resonant cavities. For the considered filters, it is checked that very close maximum values of the electric field magnitude are reached in their respective middle cavities, equal to 23 548 V/m and 23 434 V/m in the RW and GGW cases for an input power level of 1 W. Additionally, and as would be expected from the previous design work performed in sections II and III, the computed MP threshold levels are also in the measurable power range of the available facility.

In Fig. 19 we show the electron cloud distributions inside the two inductive filters, considering in each case (as the input power level) the predicted MP threshold value for the measured SEY data (see Table 5). In both cases, and at 17.4 GHz (the center frequency of the two measured responses), it can be seen that the RF discharge occurs within the middle resonator, where the electric field intensity is higher (as expected for odd-order filters). From such results for the GGW filter case, and as it was anticipated in section III for the employed zero-gap realization (with an air gap below 20 μm), MP breakdown is clearly avoided in the critical areas above the metal pins, even at the high frequency range (Ka-band) considered in this work.

For validation purposes, a MP test campaign (of both RW and GGW filter prototypes) was completed (according to the standard setup compiled in [44]) at the European High Power RF Space Laboratory [33]. The test bed used for the MP test campaign of both the RW and GGW filters is shown in Fig. 20. The MP tests were performed just right after the previously cited SEY measurements (of aluminium material) were done, in order to avoid undesired aging effects. As can be seen in Table 5, the MP threshold simulated results (using the experimental SEY data) are remarkably similar to the corresponding measured data, thus revealing the convenience of using more realistic SEY values (of involved materials) in advanced MP simulation tools.

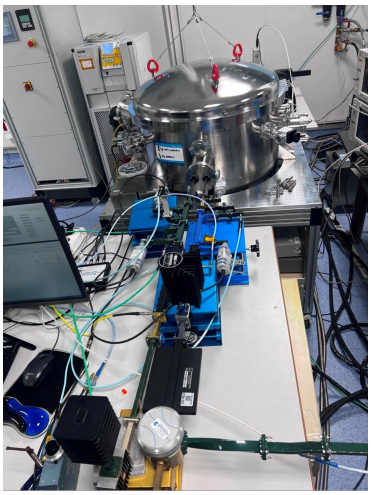

(*a*)

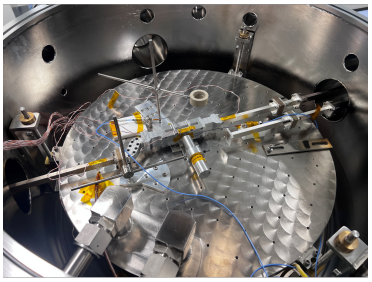

(*b*)

FIGURE 20. External part of the MP test bed in (a), and GGW filter installed in the thermal vacuum chamber in (b).

It must be also noted that the MP experimental results are also very close for both technological realizations (RW and GGW) of the considered inductive filters (with the same internal height of 3 mm, effectively selected to match requirements for standard-size components and measurable MP breakdown power levels). This promising result also confirms that the used zero-gap realization (with machining accuracy levels around 20 μm) can also provide MP-free real components at higher frequencies (17-18 GHz), thus encouraging its potential use in Ka-band satellite communication payloads. Previous MP results for the zero-gap GGW technology can only be found for simpler structures than filters (i.e. GGW uniform sections) and operating at lower frequencies (X-band) [32]. Furthermore, the proposed zero-gap GGW solution does not need of an optimized design of the involved bed of metal pins (including a related parametric analysis), as it was the case for a recent work on a different discharge effect (corona) using the standard (non-zero gap) GGW approach [31].

V. CONCLUSIONS

In this work, a comparative study (based on theoretical and experimental results) of the MP effect for inductively coupled bandpass filters, realized in both the classical RW and the latest GGW technologies, is fully detailed. For that purpose, two filter units operating in the frequency range (17-18 GHz) planned for Ka-band satellite communications have been considered. For the effective design of the RW and GGW filters, meeting realistic size and electrical specifications together with measurable MP breakdown levels, very efficient modeling tools of such a discharge effect in RWs have been successfully applied. Then, more accurate results validating the MP response of the two given filter geometries, have been computed with a commercially available code for tracking charged particles inside microwave components.

The two designed filter prototypes, composed of a body with the considered inductive topology and a top metal lid, have been manufactured with an internal milling technique offering a dimensional accuracy of 20 μm. For the GGW case, the zero-gap technological realization (including a potential very small air gap above the metal pins due to the cited tolerance) has been implemented. Before completing a standard MP test campaign of the two filter prototypes, SEY experimental results for the real employed material (aluminium) have also been procured, and then used to perform more realistic simulations of the considered discharge effect.

The measured results for MP threshold values in both RW and GGW filter samples, are very similar to those predicted by precise simulators incorporating the experimental SEY data. Thus, an important conclusion is reached on the relevance of using real SEY data for the employed material, which allows a very accurate modelling of the MP discharge effect with available software products. Another major outcome of the study performed (fully validated with experimental data of real hardware), is that bandpass filters properly realized in the zero-gap GGW technology have very large MP threshold power levels. In fact, such results are shown to be very close to those of the equivalent -same height- RW counterpart, thus confirming the practical use of GGW filters in real space applications operating at the most challenging Ka-band frequency range.

REFERENCES

[1] A. J. Hatch and H. B. Williams, "Multipacting modes of high-frequency gaseous breakdown", *Phys. Rev.*, vol. 112, pp. 681-685, Nov. 1958.
[2] J. R. M. Vaughan, "Multipactor", *IEEE Trans. Electron Devices*, vol. 35, no. 7, pp. 1172-1180, Jul. 1988.
[3] J. R. M. Vaughan, "A new formula for secondary emission yield," *IEEE Trans. Electron Devices*, vol. 36, no. 9, pp. 1963-1967, Sept. 1989.
[4] W.C. Tang and C. M. Kudsia, "Multipactor breakdown and passive intermodulation in microwave equipment for satellite applications," in *Proc. IEEE Conf. Mil. Commun.*, Oct. 1990, pp. 181–187
[5] M. Jimenez, B. Gimeno, C. Miquel-Espanya, D. Raboso, S. Anza, C. Vicente, J. Gil, F. Pereira, A. Melcón, M. Taroncher, M. Reglero, and V.E. Boria, "Analysis of the electromagnetic radiation generated by a multipactor discharge occurring within a microwave passive component," *J. Phys. D, Appl. Phys.*, vol. 43, no. 39, Oct. 2010, Art. no. 395501.
[6] D. Raboso, "Introduction to high power RF breakdown effects and PIM," in *Proc. Workshop High Power RF Breakdown PIM Space Appl., 48th Eur. Microw. Conf.*, Madrid, Spain, Sep. 2018.
[7] R. J. Cameron, C. M. Kudsia, and R. R. Mansour, *Microwave Filters for Communication Systems: Fundamentals, Design, and Applications*, 2nd ed. Hoboken, NJ, USA: Wiley, 2018.
[8] J. Uher, J. Bornemann, and U. Rosenberg, *Waveguide Components for Antenna Feed Systems: Theory and CAD*. Artech House, 1993.

[9] D. Raboso, "Multipactor effect on board spacecrafts: present situation, future research activities and testing capabilities at the European Space Agency," in *Proc. Int. Vacuum Electronics Conf.*, pp. 14.2-14.4, 2000.

[10] J. Galarza, J. Navaridas, J. Pascual, T. Romero, J. Munoz, and I. Bustinduy, "Parallelizing multipacting simulation for the design of particle accelerator components," in *2023 31st Euromicro Int. Conf. on Parallel, Distributed and Network-Based Process (PDP)*, in 2023, pp. 149–153.

[11] A. Woode and J. Petit, "Diagnostic investigations into the multipactor effect, susceptibility zone measurements and parameters affecting a discharge," ESA/ESTEC, Noordwijk, The Netherlands, Work. Paper 1556, Nov. 1989.

[12] V.E. Semenov, E.I. Rakova, D. Anderson, M. Lisak, and J. Puech, "Multipactor in rectangular waveguides," *Phys. Plasmas*, vol. 14, no. 3, Mar. 2007, Art. no. 033501.

[13] A. M. Pérez, V. E. Boria, B. Gimeno, S. Anza, C. Vicente, and J. Gil, "Multipactor analysis in circular waveguides," *J. Electromagn. Waves Appl.*, vol. 23, nos. 11–12, pp. 1575–1583, 2009.

[14] D. Gonzalez-Iglesias, P. Soto, S. Anza, B. Gimeno, V.E. Boria, C. Vicente, and J. Gil, "Multipactor susceptibility charts for ridge and multiridge waveguides," *IEEE Trans. Electron Devices*, vol. 59, no. 12, pp. 3601–3607, Dec. 2012.

[15] A.M. Perez, C. Tienda, C. Vicente, S. Anza, J. Gil, B. Gimeno, V.E. Boria, and D. Raboso, "Prediction of multipactor breakdown thresholds in coaxial transmission lines for traveling, standing, and mixed waves," *IEEE Plasma Sci.*, vol. 37, no. 10, pp. 2031–2040, Oct. 2009.

[16] V.E. Semenov, E. Rakova, A. Sazontov, I.M. Nefedov, V.I. Pozdnyakova, I.A. Shereshevskii, D. Anderson, M. Lisak, and J. Puech, "Simulations of multipactor thresholds in shielded microstrip lines," *J. Phys. D, Appl. Phys.*, vol. 42, no. 20, Sep. 2009, Art. no. 205204.

[17] P. Gonzalez, C. Alcaide, R. Cervera, M. Rodríguez, O. Monerris, J. Petit, A. Rodríguez, A. Vidal, J. Vague, J.V. Morro, P. Soto, and V.E. Boria, "Multipactor threshold estimation techniques based on circuit models electromagnetic fields and particle simulators", *IEEE J. Microw.*, vol. 2, no. 1, pp. 57-77, Jan. 2022.

[18] H. Fenech, S. Amos, A. Tomatis, and V. Soumpholphakdy, "High throughput satellite systems: An analytical approach", *IEEE Trans. Aerosp. Electron. Syst.*, vol. 51, no. 1, pp. 192-202, Jan. 2015.

[19] J. Christensen, "ITU regulations for Ka-band satellite networks," in *Proc. 30th AIAA Int. Commun. Satell. Syst. Conf. (ICSSC)*, Sep. 2012, p. 15179. [Online]. Available: https://arc.aiaa.org/doi/abs/10.2514/6.2012-15179

[20] E. Rajo-Iglesias and P.-S. Kildal, "Groove gap waveguide: A rectangular waveguide between contactless metal plates enabled by parallel-plate cutoff," in *Proc. 4th Eur. Conf. Antennas Propag.*, Barcelona, Spain, Apr. 2010, pp. 1–4.

[21] L. Wu, Y. Wu, Y. Yao, R. Huang, Z. Xu and W. Wang, "Dual-band bandpass filter with controllable transmission zeros using multimode GGW cavity," *IEEE Microw. Wireless Technol. Lett.*, vol. 34, no. 7, pp. 891-894, Jul. 2024.

[22] M. Malki, L. Yang and R. Gomez-Garcia, "Sharp-rejection in-line groove-gap-waveguide bandpass filter with multiple transmission zeros for ku-band application," *IEEE Microw. Wireless Technol. Lett.*, vol. 34, no. 5, pp. 478-481, May 2024.

[23] Q. Li, D. Guo, J. Mou, J. Li and K. -D. Xu, "Groove gap waveguide bandpass filter based on spoof surface plasmon polariton for ka-band applications," *IEEE Trans. Microw. Theory Tech.*, vol. 72, no. 1, pp. 340-347, Jan. 2024.

[24] Z. Liu, J. -Y. Deng and D. Sun, "Slow-wave groove gap waveguide bandpass filter," *IEEE Access*, vol. 7, pp. 52581-52588, 2019.

[25] S. Marini, M. Ferrando Rocher, A. Morales Hernández, E. Gimeno Nieves, A. Jorge López and V . E. Boria, "Ka-band diplexer design based on half-mode groove gap waveguide," *Int. J. Electron. Commun.*, vol. 175, no. 1, pp. 1434-8411, Feb. 2024.

[26] P.-S. Kildal, E. Alfonso, A. Valero-Nogueira, and E. Rajo-Iglesias, "Local metamaterial-based waveguides in gaps between parallel metal plates," *IEEE Antennas Wireless Propag. Lett.*, vol. 8, pp. 84–87, 2009.

[27] E. Rajo-Iglesias and P. S. Kildal, "Numerical studies of bandwidth of parallel-plate cut-off realised by a bed of nails, corrugations and mushroom-type electromagnetic bandgap for use in gap waveguides," *IET Microw., Antennas Propag.*, vol. 5, no. 3, p. 282—289, Feb. 2011.

[28] A. Berenguer, D. Sánchez-Escuderos, B. Bernardo-Clemente, M. Baquero-Escudero, and V.E. Boria, "Groove gap waveguide as an alternative to rectangular waveguide for H-plane components," *Electron. Lett.*, vol. 52, no. 11, pp. 939–941, May 2016.

[29] M. Baquero-Escudero, A. Valero-Nogueira, M. Ferrando-Rocher, B. Bernardo-Clemente, and V.E. Boria-Esbert, "Compact combline filter embedded in a bed of nails," *IEEE Trans. Microw. Theory Techn.*, vol. 67, no. 4, pp. 1461–1471, Apr. 2019.

[30] E. Rajo-Iglesias, M. Ferrando-Rocher, and A. U. Zaman, "Gap waveguide technology for millimeter-wave antenna systems," *IEEE Commun. Mag.*, vol. 56, no. 7, pp. 14–20, 2018.

[31] A. Morales-Hernández, M. Á. Sánchez-Soriano, M. Ferrando-Rocher, S. Marini, and V.E. Boria, "In-depth study of the corona discharge breakdown thresholds in groove gap waveguides and enhancement strategies for inductive bandpass filters," *IEEE Access*, vol. 10, pp. 129 149–129 162, 2022.

[32] J. Vague, I. Asensio, Á. Coves, Á. San Blas, M. Reglero, A. Vidal, D. Raboso, M. Baquero-Escudero, and V.E. Boria, "Study of the multipactor effect in groove gap waveguide technology," *IEEE Trans. Microw. Theory Tech.*, vol. 70, no. 5, pp. 2566–2578, May 2022.

[33] European Space Agency and Val Space Consortium-European Space Agency High-Power Laboratories, Valencia, Spain. [Online]. Available: www.val-space.com

[34] M. Guglielmi, A. Alvarez, and G. Gheri, "Multimode synthesis procedure for microwave filters based on thick inductive windows," in *IEEE MTT-S Int. Microwave Symp.*, Atlanta, GA, USA, 1993, pp. 447–450.

[35] M. Guglielmi, "Simple CAD procedure for microwave filters and multiplexers," *IEEE Trans. Microw. Theory Tech.*, vol. 42, no. 7, pp. 1347–1352, Jul. 1994.

[36] CST Microwave Studio. [Online]. Available: https://www.3ds.com/products/simulia/cst-studio-suite

[37] C. Vicente, M. Mattes, D. Wolk, B. Mottet, H.L. Hartnagel, J.R. Mosig, and D. Raboso, "Multipactor breakdown prediction in rectangular waveguide based components," in *IEEE MTT-S Int. Microw. Symp. Dig.*, Jun. 2005, pp. 1055–1058.

[38] A. Berenguer, Á. Coves, F. Mesa, E. Bronchalo, and B. Gimeno, "Analysis of multipactor effect in a partially dielectric-loaded rectangular waveguide," *IEEE Trans. Plasma Sci.*, vol. 47, no. 1, pp. 259–265, Jan. 2019.

[39] A. Berenguer, Á. Coves, B. Gimeno, E. Bronchalo, and V.E. Boria, "Experimental study of the multipactor effect in a partially dielectric-loaded rectangular waveguide," *IEEE Microw. Wireless Compon. Lett.*, vol. 29, no. 9, pp. 595–597, Sep. 2019.

[40] *Multipacting Design and Test*, document ECSS-E-ST-20-01C, European Cooperation for Space Standarization (ECSS), ESA-ESTEC, ESA Publication Division, Amsterdam, The Netherlands, Jun. 2020.

[41] A. Berenguer, V. Fusco, D. E. Zelenchuk, D. Sánchez-Escuderos, M. Baquero-Escudero, and V.E. Boria-Esbert, "Propagation characteristics of groove gap waveguide below and above cutoff," *IEEE Trans. Microw. Theory Techn.*, vol. 64, no. 1, pp. 27–36, Jan. 2016.

[42] A. Tamayo-Domínguez, J.-M. Fernández-González, and M. Sierra-Pérez, "Groove gap waveguide in 3-D printed technology for low loss, weight, and cost distribution networks," *IEEE Trans. Microw. Theory Tech.*, vol. 65, no. 11, pp. 4138–4147, Nov. 2017.

[43] S. Cogollos, J. Vague, V.E. Boria, and J. D. Martínez, "Novel planar and waveguide implementations of impedance matching networks based on tapered lines using generalized superellipses," *IEEE Trans. Microw. Theory Techn.*, vol. 66, no. 4, pp. 1874–1884, Apr. 2018.

[44] *Multipacting Handbook*, document ECSS-E-HB-20-01A, European Cooperation for Space Standarization (ECSS), ESA-ESTEC, ESA Publication Division, Amsterdam, The Netherlands, Jun. 2020.

ALEJANDRO JORGE LÓPEZ was born in Murcia, Spain in December 1996. He graduated from Universidad Politécnica de Cartagena (UPCT, Spain) in 2019 with a BSc in Telecommunication Systems, and he is currently pursuing an MSc in Telecommunication Engineering at Universitat Politècnica de València (UPV, Spain). From 2019 to 2021, he worked as a researcher in the integration of innovative technologies, including artificial intelligence (AI), business intelligence (BI) and cognitive vision. Later on, he worked as a cloud engineer to implement AI, BI and cloud computing technologies for renewable energy industries. He is currently working as a research engineer at the Institute of Telecommunications and Multimedia Applications (iTeam), within the Microwave Applications Group (GAM), developing new solutions for satellite communication payloads (novel topologies for microwave filters) and for Ground Stations (based on Software Defined Radio, SDR). His main research interests include Ground Station, CubeSats, SDR, Multipactor, microwave filters, and high-power effects.

JOAQUÍN VAGUE was born in Valencia, Spain, in 1970. He received the degree in electronic engineering from the Universitat de Valencia, Valencia, in 2003. He is currently pursuing the Ph.D. degree in electronic engineering. He is currently a Technical Researcher in charge of several laboratories with the Departamento de Comunicaciones, Universitat Politecnica de Valencia (UPV), Valencia. His current research interests include the design of microwave passive devices, especially in filters and nonreciprocal devices and the improvement in manufacturing processes in the RF and microwave range.

IRENE ASENSIO was born in Segorbe (Castellón), Spain, in 1999. She is currently pursuing the degree in Telecommunications Engeneering. Her current research interests include the design of microwave passive devices, especially in filters and nonreciprocal devices and the improvement in manufacturing processes in the RF and microwave range.

ANGELA COVES (S'04–A'06–M'10) received the Licenciado and Ph.D. degrees in physics from the Universidad de Valencia, Valencia, Spain, in 1999 and 2004, respectively. In 2001, she joined the Departamento de Ingeniería de Comunicaciones, Universidad Miguel Hernández de Elche, Elche, Spain, where she became a Full Professor in 2021. Her current research interests include the analysis and design of microwave passive components, periodic structures, and RF breakdown high power effects.

ÁNGEL ANTONIO SAN-BLAS was born in Fortaleny, Valencia, Spain, in 1976. He received the Ingeniero de Telecomunicación and the Doctor Ingeniero de Telecomunicación degrees from the Universitat Politècnica de València, Valencia, Spain, in 2000 and 2008, respectively. From 2001 to 2002, he was a Researcher Assistant with the Departamento de Comunicaciones, Universitat Politècnica de València, where he was involved in the development of simulation tools for the analysis and design of waveguide devices. From November 2001 to March 2002, he was a Researcher with the Department of Electronics, Università degli Studi di Pavia, Pavia, Italy, where he was involved in the research project MillimeterWave and Microwave Components Design Framework for Ground and Space Multimedia Network (V European Framework Project). Since 2003, he has been an Associate Professor with the Departamento de Ingeniería de Comunicaciones, Universidad Miguel Hernández de Elche, Elche, Spain. His current research interests include the analysis and design of passive waveguide components for satellite communication systems. Dr. San-Blas also serves as an Editorial Board Member (Area Editor) for the International Journal of Electronics and Communications (Elsevier).

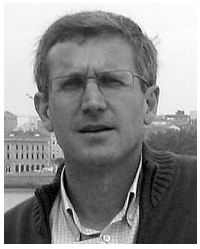

MARIANO BAQUERO-ESCUDERO (S'87–M'90) was born in Murcia, Spain, on January 11, 1962. He received the Telecommunications Engineering degree from the Polytechnic University of Catalonia (UPC), Barcelona, Spain, in 1986, and the Ph.D. degree from the Universitat Politècnica de València (UPV), València, Spain, in 1994. From 1986 to 1988, he was with the Antennas, Microwave and Radar Group, UPC, where he was involved with the development of a cylindrical nearfield facility to measure a 3-D radar antenna in CESELSA. Since 1989, he has been with the UPV, where he became a Full Professor in 2003. During 1995, he held a postdoctoral grant with the Joint Research Centre, European Commission, Ispra, Italy, where he developed high-resolution algorithms for radar applications. From April 1996 to February 1998, he was a Vice-Dean of the Telecommunications Engineering School of Valencia. He is currently with the Communications Department and the Institute of Telecommunications and Multimedia Application, Universitat Politècnica de València. His main research interests include microwave circuit and antenna analysis, design, and measurement.

MÁRIAM TARONCHER was born in Alicante, Spain, in 1982. She received the Ingeniería de Telecomunicaciones degree from the Universitat Politècnica de València (UPV), Valencia, Spain, in 2008. From 2006 to 2008, she was a Fellow Researcher with the Institute of Telecommunications and Multimedia Applications (iTEAM), Universitat Politècnica de València (UPV), and the Department of Applied Physics Electromagnetism, Institute of Materials Science (ICMUV), Universitat de València (UVEG), Valencia. Since 2008, she has been a Technical Researcher with the iTEAM, UPV. Since 2010, she has been a Laboratory Engineer with European Space Agency (ESA), Val Space Consortium (VSC), Valencia. Her current research interests include the analysis of effects of high-power microwave devices.

ANA VIDAL PANTALEONI (M'01) was born in Valencia (Spain) in 1970. She received the Telecommunications Engineer degree from the Universidad Politécnica de Valencia (Spain) and she stayed one year at University of Strathclyde, Glasgow (U.K.), under the Erasmus international exchange program. In 1993, she was involved in broadband communications development in the main research center of Telecom Portugal. She then became a Research Assistant with the Universidad Politécnica de Valencia. In 1995 and 1996, she held a Spanish Trainee position with the European Space research and Technology Centre (ESTEC)–European Space Agency (ESA), Noordwijk, The Netherlands, where she was involved in the study and implementation of software for synthetic aperture radar (SAR) image processing. In 1996, she returned to the Universidad Politécnica de Valencia, where she held several lecturing positions, and became an Associate Professor in 2001. Her current interests are Remote Sensing data classification, GNSS algorithms and numerical methods for microwave structures analysis, including high power effects.

VICENTE E. BORIA (S'91–A'99–SM'02-F'18) was born in Valencia, Spain in 1970. He received his "Ingeniero de Telecomunicacion" degree (with´ first-class honors) and the "Doctor Ingeniero de Telecomunicacion" degree from the Universidad´ Politecnica de Valencia, Valencia, Spain, in 1993´ and 1997, respectively. In 1993, he joined "Departamento de Comunicaciones", Universidad Politecnica de Valencia, where he has been Full Professor since 2003. In 1995 and 1996, he was holding a Spanish Trainee position with the European Space Research and Technology Centre, European Space Agency (ESTEC-ESA), Noordwijk, The Netherlands, where he was involved in the area of EM analysis and design of passive waveguide devices. He has authored or co-authored 15 chapters in technical textbooks, 200 papers in refereed international technical journals, and over 250 papers in international conference proceedings. His current research interests are focused on the analysis and automated design of passive components (in particular filters and multiplexers), as well as on the simulation and measurement of power effects in high-frequency devices and systems. Prof. Boria has been a member of the IEEE Microwave Theory and Techniques Society (IEEE MTT-S) and the IEEE Antennas and Propagation Society (IEEE AP-S) since 1992. He acts as a regular reviewer of the most relevant IEEE and IET technical journals on his areas of interest. He has been Associate Editor of IEEE Microwave and Wireless Components Letters (2013-2018) and IET Electronics Letters (2015-2018). Presently, he serves as Subject Editor (Microwaves) of IET Electronics Letters, and as Editorial Board member of International Journal of RF and Microwave Computer-Aided Engineering. He is also member of the Technical Committees of the IEEEMTT International Microwave Symposium and of the European Microwave Conference.